Journal of Orthopaedic Translation 55 (2025) 309–322

Contents lists available at ScienceDirect

Journal of Orthopaedic Translation

journal homepage: www.journals.elsevier.com/journal-of-orthopaedic-translation

Original article

Epigenetic reprogramming via EZH2 inhibition rescues fibroadipose pathogenesis in secondary lymphedema through activating PPARγ signaling

Ziyu Chen [a,b,1], Zhi Yao [a,1], Mengfan Wu [c,1], Yuluan Wu [a], Jianlin Zhang [d], Zhuangyao Liao [a], Junyu Qian [a], Jiewen Wei [a,e], Lili Song [f], Longbiao Yu [f], Jingjing Wen [f], Zhegang Zhou [f], Yihao Wei [g], Yuefeng Yao [a], Zetao Ma [a], Pei Liu [a], Shailesh Agarwal [b], Ye Li [g,***], Lixiang Xue [d,**], Deli Wang [a,*]

[a] Department of Bone and Joint Surgery, Peking University Shenzhen Hospital, Shenzhen Peking University-The Hong Kong University of Science and Technology Medical Center, Shenzhen, Guangdong, China
[b] Department of Surgery, Brigham and Women's Hospital and Harvard Medical School, Boston, MA, USA
[c] Department of Plastic Surgery, Peking University Shenzhen Hospital, Shenzhen, Guangdong, China
[d] Cancer Center of Peking University Third Hospital, Center of Basic Medical Research, Institute of Medical Innovation and Research, Peking University Third Hospital, Beijing, China
[e] Shantou University Medical College, Shantou, Guangdong, China
[f] Department of Hand and Microsurgery, Peking University Shenzhen Hospital, Shenzhen, Guangdong, China
[g] Department of Rehabilitation Sciences, The Hong Kong Polytechnic University, Hong Kong Special Administrative Region of China

ARTICLE INFO

Keywords:
Secondary lymphedema
EZH2
Fibroadipose tissue
PPARγ
AdMSCs

ABSTRACT

Background: Secondary lymphedema, a progressive disorder characterized by pathological fibroadipose tissue accumulation, is a common problem after cancer treatment and orthopedic surgery. It remains a therapeutic enigma due to its self-perpetuating fibrotic cascade and lack of disease-modifying therapies. While current therapeutic approaches focus on symptom management and volume reduction, they don't address the epigenetic reprogramming driving fibrotic commitment—a process recently linked to enhancer of zeste homolog 2 (EZH2). Although EZH2 inhibitor EPZ6438 has been approved for clinical application, its therapeutic potential in fibroadipose pathogenesis remains unexplored, leaving a critical gap in understanding epigenetic factors in lymphedema progression.

Methods: Human skin tissue was collected from lymphedema patients and normal controls. Histological/immunofluorescence staining and RNA sequencing were performed. In vivo, a mouse hind limb secondary lymphedema model was established by lymphadenectomy. EZH2 inhibitors (EPZ6438, GSK126) were intraperitoneally injected. Skin samples were collected for histological assessment and immuno-staining. In vitro, adipose-derived mesenchymal stem cells (AdMSCs) were treated with transforming growth factor beta 1 (TGFβ1) and EZH2 inhibitors. Western blot, RT-qPCR and ChIP-qPCR were carried out.

Results: Fibrous tissue was observed in lymphedema samples, with concomitant elevation of EZH2 and H3K27me3 levels in the nucleus. RNA sequencing and gene set enrichment analysis (GSEA) revealed significant downregulation of the peroxisome proliferator-activated receptor (PPAR) signaling in lymphedema tissue. Pharmacological inhibition of EZH2 significantly attenuated cutaneous thickening, fibroadipose layer expansion, and collagen deposition in the mouse lymphedema model. PPARγ was induced while phospho-SMAD2/3

* Corresponding author. Department of Bone and Joint Surgery, Peking University Shenzhen Hospital, Shenzhen Peking University-The Hong Kong University of Science and Technology Medical Center, 1120 Lianhua Rd, Shenzhen, 518000, Guangdong, China.
** Corresponding author. Cancer Center of Peking University Third Hospital, Center of Basic Medical Research, Institute of Medical Innovation and Research, Peking University Third Hospital, Beijing, 100191, China.
*** Corresponding author. Department of Rehabilitation Sciences, The Hong Kong Polytechnic University, 999077, Hong Kong Special Administrative Region of China.
E-mail addresses: yeli@link.cuhk.edu.hk (Y. Li), lixiangxue@hsc.pku.edu.cn (L. Xue), wangdelinavy@163.com (D. Wang).
[1] These authors contributed equally to this work.

https://doi.org/10.1016/j.jot.2025.08.014
Received 25 April 2025; Received in revised form 15 August 2025; Accepted 25 August 2025
Available online 1 October 2025

activation was suppressed. In TGFβ1 stimulated AdMSCs, EZH2 inhibition upregulated PPARγ expression and inhibited fibrogenic differentiation of the cells.
Conclusion: EZH2 inhibitors exerted potent anti-fibrotic effects in secondary lymphedema though activating PPARγ signaling, offering novel insights and strategies for fibrotic disorders.
The translational potential of this article: This study demonstrated that targeted inhibition of the EZH2-PPARγ axis effectively inhibited fibrogenic differentiation of AdMSCs and reduced fibroadipose tissue in secondary lymphedema, indicating it is a promising strategy for secondary lymphedema treatment, offering novel insights and strategy for musculoskeletal fibrotic disorders.

1. Introduction

Lymphedema, a chronic and progressive condition characterized by abnormal accumulation of protein-rich lymphatic fluid and fibroadipose tissue in the extremities, affects more than 250 million people around the world [1,2]. Secondary lymphedema is more common than primary lymphedema. It is caused by the damage to the lymphatic system after trauma, recurrent infection and radiation therapy [3,4]. While the musculoskeletal system contains an extensive lymphatic network, emerging evidence suggests that secondary lymphedema may occur after common orthopedic surgery, including musculoskeletal tumors resection and joint arthroplasty [5–7]. It has detrimental impact on clinical outcomes including poor wound healing, increased risk of infection, and prolonged recovery time, while fibrous tissue can causes joint stiffness and affects joint function [8]. An increasing number of orthopedic surgeons are recognizing the high prevalence of lymphedema in orthopedic practice.

The International Society of Lymphology (ISL) staging system (0 - III) was used to standardize the stages of lymphedema. In stage 0, swelling is not yet visible, but the lymph system may be compromised already. Visible swelling begins in stage I, often reducing with elevation. Swelling becomes more persistent in stage II, and tissue starts to harden. In stage III, notable subcutaneous tissue hyperplasia and fibrosis occur. Conservative treatments are often applied to patients from stage 0 to stage II. Surgical intervention will be considered for stage III patients. Current therapeutic strategies focus on symptom management and volume reduction. Complete decongestive therapy (CDT) shows great therapeutic efficacy for early-stage patients. But it requires long-term adherence to daily compression (more than 12 h a day), and the compliance rate is low [9,10]. Surgical interventions performed by orthopedic and plastic surgeons, including vascularized lymph node transfer (VLNT) and liposuction, have also demonstrated efficacy in select advanced-stage patients [11,12]. However, these surgeries may result in surgical complications including infections, delayed wound healing, and lymphatic leakage [13]. The evolution of microsurgical techniques has significantly expanded the application of lymphaticovenular anastomosis (LVA) in secondary lymphedema management, and a growing number of patients have undergone this procedure as a first surgical intervention. However, the long-term therapeutic efficacy and durability of LVA remain to be comprehensively validated through extended follow-up studies. Moreover, these approaches don't address the underlying fibrotic pathology and progressive collagen deposition.

The accumulated lymph fluid can stimulate the excessive synthesis of collagen fibers, which can cause thickening of skin tissue, and further affect the transport capacity of the lymphatic system, thereby aggravating lymphedema and forming a vicious circle [14,15]. Anti-fibrotic intervention should be initiated and sustained throughout disease progression to prevent irreversible fibrotic consolidation. However, current anti-fibrotic approaches remained limited and were often adjunctive. Compression therapy remains the cornerstone of lymphedema management, while recent innovations including multi-layer systems and high-pressure intermittent compression focus on optimizing pressure distribution. Thermal therapies such as microwave and far-infrared radiation also demonstrate good potential. These treatments still fail to completely stop the progression of fibrosis. Anti-inflammatory pharmacological agents including Ketoprofen, a nonsteroidal anti-inflammatory drug (NSAID), and tacrolimus, an anti-T-cell agent, were examined to treat lymphedema [16,17]. These drugs target the inflammation of the disease rather than the fibrotic process directly. Transforming growth factor-beta (TGFβ) is an essential regulator of fibrosis that increases collagen production and promotes ECM deposition. Accumulating evidence indicates that dysregulated activation of the TGFβ-SMAD2/3 pathway plays a pivotal role in the progression of fibroadipose pathogenesis in secondary lymphedema [18,19]. However, there are no Food and Drug Administration (FDA)-approved anti-fibrotic drugs for the treatment of lymphedema. Therefore, novel therapeutics targeting fibrosis-specific pathways are needed to improve long-term outcomes.

Epigenetic regulation encompasses heritable, reversible modifications of chromatin structure that control gene expression without altering the DNA sequence, playing fundamental roles in cell differentiation and disease pathogenesis. This regulation is catalyzed by specialized enzymes including DNA methyltransferases (DNMTs), ten-eleven translocation (TET) enzymes, histone acetyltransferases, histone deacetylases, histone methyltransferases, histone Demethylases, etc [20]. Enhancer of zeste homolog 2 (EZH2) is a histone methyltransferase, serving as the catalytic subunit of the polycomb repressive complex 2 (PRC2) that specifically catalyzes the trimethylation of lysine 27 on histone H3 (H3K27me3), leading to transcriptional repression [21]. Emerging evidences have suggested that epigenetic regulator EZH2 may serve as a therapeutic target for fibrosis. Recent studies have unveiled the role of EZH2 in the progression of liver fibrosis [22,23], pulmonary fibrosis [24,25], renal fibrosis [26], cardiac fibrosis [27,28], and peritoneal fibrosis [29]. However, the mechanism of lymphedema fibroadipose pathogenesis might be different from visceral fibrosis, and the role of EZH2 in skin fibrosis has not been reported yet. EPZ6438 and GSK126 are potent and highly selective EZH2 methyltransferase inhibitors. GSK126 has been most widely used as EZH2 inhibitors in research [30]. Furthermore, EPZ6438 has been approved by FDA of the United States for the treatment of lymphoma, it may be a potential treatment for secondary lymphedema [31,32].

In this study, we demonstrated the upregulation of EZH2 in human lymphedema fibroadipose tissue, examined the therapeutic effect of the EZH2 inhibitors on experimental secondary lymphedema model in mice and explored the possible mechanism. Furthermore, we investigated the role of EZH2 inhibition in the fibrogenic differentiation of adipose-derived mesenchymal stem cells (AdMSCs).

2. Materials and methods

2.1. Human skin samples

Human samples were collected in accordance with the protocol approved by Peking University Shenzhen Hospital (No. 2025-047). The protocol used in this study was compliant with the ethical guidelines of the Helsinki Declaration. Written informed consent was obtained from all patients. Lymphedema skin tissues were collected from patients diagnosed with secondary lymphedema in ISL stage III and underwent tissue resection surgery in department of orthopaedics (Table S1). Normal control skin tissues were collected from patients who underwent

plastic surgery. The collected tissues were used for cell isolation, or fresh frozen by liquid nitrogen and stored at −80 °C fridge, or fixed in 4 % paraformaldehyde solution for further examination.

2.2. Animal studies

Animal experiments adhered to the Guidelines for the Care and Use of Laboratory Animals and were approved by the Institutional Animal Care and Use Committee (IACUC) of Peking University Shenzhen Hospital (No. 2024-315). Male and female C57BL/6J mice (6–8 weeks old, weight: 23 ± 2 g) were obtained from BesTest Bio-Tech (Zhuhai, China) and acclimatized for 1 week in the Shenzhen Peking University-Hong Kong University of Science and Technology Medical Center vivarium. All mice were housed under standard laboratory conditions with a 12 h light/dark cycle, ambient temperature of 25 °C, and humidity of 50 %.

A total of 24 male mice and 24 female mice were randomly assigned into 4 groups (6 male mice and 6 female mice per group) as follows: (1) Sham + Vehicle group received sham operation and injected with vehicle, (2) LN + Vehicle group received lymphadenectomy surgery and injected with vehicle, (3) LN + EPZ6438 group received lymphadenectomy surgery and injected with EPZ6438, (4) LN + GSK126 group received lymphadenectomy surgery and injected with GSK126. For rescue experiment, A total of 24 male mice were randomly assigned into 4 groups (n = 6 per group) as follows: (1) Sham + Vehicle group received sham operation and injected with vehicle, (2) LN + Vehicle group received lymphadenectomy surgery and injected with vehicle, (3) LN + EPZ6438 group received lymphadenectomy surgery and injected with EPZ6438, (4) LN + EPZ6438 + GW9662 group received lymphadenectomy surgery and injected with EPZ6438 and GW9662.

Mice hind limb secondary lymphedema model was established as previously described [33]. Briefly, the ipsilateral superficial inguinal, popliteal, and deep inguinal lymph nodes and the femoral lymphatic vessel in the hind limb were surgically excised. EPZ6438 (Selleck Chemical, S7128, TX, USA) and GSK126 (Selleck Chemical, S7061, TX, USA) were dissolved in DMSO at the concentration of 50 mg/mL and was diluted in corn oil to the final concentration of 5 mg/mL before injection. GW9662 (Selleck Chemical, S2915, TX, USA) was first prepared as a 25 mg/mL stock solution in DMSO, which was further diluted with corn oil to the final concentration of 1.25 mg/mL prior to injection. Vehicle consists of same amount of DMSO and coin oil. Mice were intraperitoneally injected with vehicle or EPZ6438 (50 mg/kg) or GSK126 (50 mg/kg) on day 1 and day 4 after the surgery. GW9662 (5 mg/kg) was used in the rescue experiment on day 4 after the surgery. All mice were sacrificed on day 7. Hind limb skin and muscle samples were harvested and fixed in 4 % paraformaldehyde solution for further examination.

2.3. Tissue embedding and section

After fixation for 48 h, tissues were dehydrated, embedded in paraffin. Serial 5-μm-thick sections were obtained and subjected to histological/immunofluorescence staining.

2.4. Histological analysis

Hematoxylin and eosin (H&E), Picrosirius red and Masson's trichrome staining were carried out according to the manufacturer's protocol. Images were captured by using Olympus BX53 microscope (UCMAD3, T7). Mice skin thickness, epidermis thickness and fibroadipose tissue thickness were assessed. Fibrosis was assessed with the image thresholding plugin in ImageJ software (Media Cybernetics, Bethesda, MD, USA). All assessment were performed by 2 independent researchers under blinded conditions.

2.5. Immunofluorescence staining

Tissue sections were deparaffinized, rehydrated, immersed in sodium citrate buffer and heated in a temperature gradient for antigen retrieval. Sections were then soaked in 3 % H_2O_2 to remove the endogenous peroxidase activity, and blocked with 10 % goat serum, 1 % bovine serum albumin (BSA), and 0.3 % Triton (Millipore Sigma) in PBS for 1 h. Primary antibodies against EZH2 (1:200), H3K27me3 (1:200), αSMA (1:200), PPARγ (1:200), p-SMAD2/3 (1:200) were incubated at 4 °C overnight. Following secondary antibodies were incubated for 1 h in the dark: Alexa Fluor Plus 488 goat anti-rabbit IgG (1:1000), Alexa Fluor Plus 488 goat anti-mouse IgG (1:1000), Alexa Fluor 594 goat anti-rabbit IgG (1:1000). Details of the antibodies were listed in Table 1. ProLong Diamond Antifade Mountant with DAPI (Invitrogen, P36971) was used to stain the nuclei and mount the samples. Fluorescent images were taken by Leica STELLARIS 5 confocal microscope at original magnification 20 × . Quantification of immunofluorescence staining was performed by using ImageJ software (Media Cybernetics, Bethesda, MD, USA). Three images were quantified and averaged for each sample.

2.6. RNA sequencing (RNA-Seq)

Total RNA was isolated and purified from human subcutaneous adipose tissues (lymphedema n = 5, normal control n = 3) using TRIzol Reagent (Invitrogen, Carlsbad, CA, USA) according to the manufacturer's protocol. NanoDrop ND-1000 (NanoDrop, Wilmington, DE, USA) was used to quantify the RNA amount and purity. The RNA integrity was assessed by Bioanalyzer 2100 (Agilent, CA, USA) with RIN number >7.0, and confirmed by electrophoresis with denaturing agarose gel. Two rounds of purification of Poly (A) RNA were carried out from 1 μg total RNA using Dynabeads Oligo$(dT)_{25}$ (Thermo Fisher, 61005, CA, USA). Poly(A) RNA was then fragmented into small pieces using Magnesium RNA Fragmentation Module (NEB, E6150, USA) under 94 °C for 5–7 min. Cleaved RNA fragments were reverse-transcribed to cDNA by using SuperScript™ II Reverse Transcriptase (Invitrogen, 1896649), which were next used to synthesize U-labeled second-stranded DNAs with *E. coli* DNA polymerase I (NEB, M0209, USA), RNase H (NEB, M0297, USA) and dUTP Solution (Thermo Fisher, R0133, USA). An A-base was added to the blunt ends of each strand for ligation to the indexed adapters. Each adapter contained a T-base overhang for ligating the adapter to the A-tailed fragmented DNA. After single- or dual-index adapters were ligated to the fragments, size selection was performed

Table 1
Antibodies for immunofluorescence staining and western blot experiments.

Antibody	Catalog#	Company
EZH2	5246	Cell Signaling Technology, Beverly, MA, USA
H3K27me3	9733	Cell Signaling Technology, Beverly, MA, USA
H3	3638	Cell Signaling Technology, Beverly, MA, USA
αSMA	48938	Cell Signaling Technology, Beverly, MA, USA
CTGF	86641	Cell Signaling Technology, Beverly, MA, USA
PPARγ	2435	Cell Signaling Technology, Beverly, MA, USA
pSMAD2/3	8828	Cell Signaling Technology, Beverly, MA, USA
SMAD2/3	8685	Cell Signaling Technology, Beverly, MA, USA
GAPDH	BL006A	Biosharp, Hefei, China
Alexa Fluor 488 goat anti-mouse IgG	BL066A	Biosharp, Hefei, China
Alexa Fluor 488 goat anti-rabbit IgG	BL067A	Biosharp, Hefei, China
Alexa Fluor 594 goat anti-rabbit IgG	BL064A	Biosharp, Hefei, China

with AMPure XP beads. U-labeled second-stranded DNAs were treated with UDG enzyme (NEB, M0280, USA), the ligated products were amplified using PCR: initial denaturation at 95 °C for 3 min; 8 cycles of denaturation at 98 °C for 15 s, annealing at 60 °C for 15 s, and extension at 72 °C for 30 s; then final extension at 72 °C for 5 min. The average insert size for the final cDNA library was 300 ± 50 bp. At last, 2 × 150 bp paired-end sequencing (PE150) was performed on the illumina Novaseq™ X Plus (LC-Bio Technology CO., Ltd., Hangzhou, China) following the vendor's recommended protocol.

2.7. Bioinformatics analysis of RNA-Seq

Fastp software (https://github.com/OpenGene/fastp) was used to remove the reads that contained adaptor contamination, low quality bases and undetermined bases with default parameter. Fastp was also used to verify the sequence quality. HISAT2 (https://ccb.jhu.edu/software/hisat2) was used to map reads to the reference genome of *Homo sapiens*. The mapped reads of each sample were assembled using StringTie (https://ccb.jhu.edu/software/stringtie) with default parameters. All transcriptomes from all samples were merged to reconstruct a comprehensive transcriptome using gffcompare (https://github.com/gpertea/gffcompare). StringTie was used to perform expression level for mRNAs by calculating FPKM (FPKM = [total_exon_fragments/mapped_reads (millions) × exon_length (kB)]). The differentially expressed mRNAs were selected with fold change >2 or <0.5 and with parametric F-test ($p < 0.05$) by R package edgeR (https://bioconductor.org/packages/release/bioc/html/edgeR.html). Functional enrichment analysis of differentially expressed genes was performed using Gene Ontology (GO) and Kyoto Encyclopedia of Genes and Genomes (KEGG) databases. Gene Set Enrichment Analysis (GSEA) was conducted to evaluate genome-wide expression profiles against predefined molecular signatures in the Molecular Signatures Database (MSigDB). The raw sequence data have been submitted to the NCBI Gene Expression Omnibus (GEO) datasets with accession number GSE302563.

2.8. Cell harvest and culture

Primary human adipose-derived mesenchymal stem cells (AdMSCs) were extracted from normal subcutaneous adipose tissue which was collected after plastic surgery. Isolation and culture of the cells were performed as previously described [34]. Briefly, the adipose tissue were minced and digested with type I collagenase (Sigma–Aldrich, 1 mg/mL) for 30 min at 37 °C. The digested tissue were filtered through a 40 μm cell strainer and centrifuged at 500g for 5 min at room temperature. Pelleted cells were washed with phosphate buffered saline (PBS) and cultured in DMEM/F12 (Gibco, C11330500BT) supplemented with 10 % fetal bovine serum (FBS, Gibco, 10099141C) and 1 % penicillin and streptomycin (Gibco, 15140122). AdMSCs were maintained at 37 °C with 5 % CO_2. Culture media was refreshed every 3 days until reaching 90 % confluence.

2.9. Cell viability and treatment

Cell viability was assessed by Cell Counting Kit-8 (CCK-8, Biosharp, BS350A, Hefei, China) according to the manufacturer's protocol. AdMSCs were seeded into 96-well plate (5000 cells per well), six replicates were set up in each group. The concentration of EPZ6438 and GSK126 used in previous studies were range from 2 μM to 20 μM in *in vitro* experiments [35,36]. Different concentration of EPZ6438 and GSK126 (0, 1, 2, 3, 4, 5, 7.5, 10, 15, and 20 μM) were administrated for 24 h and 48 h. CCK-8 solution was added and absorbance at 450 nm was measured using a microplate reader (Thermo Fisher, USA).

AdMSCs were seeded into 6-well plate (2×10^5 cells per well) and treated with/without TGFβ1 (10 ng/mL) (Peprotech, 10021) for 48 h. EPZ6438 (5 μM), GSK126 (2 μM) and GW9662 (10 μM, Selleck Chemical, S2915, TX, USA) was administrated at the same time of TGFβ1 treatment.

2.10. Reverse transcription-quantitative polymerase chain reaction (RT-qPCR)

Total RNA from human tissue and AdMSCs was isolated by using TRIzol Reagent (Invitrogen, Carlsbad, CA, USA). First-strand cDNA was synthesized by using HiScript II RT SuperMix (Vazyme, China). Real time qPCR was performed using SuperReal PreMix Plus (SYBR Green) (Tiangen, China) with Roche 480 qPCR machine according to the manufacturer's instructions. Primer sequences were listed in Table 2.

2.11. Western blotting

Proteins were extracted from AdMSCs by RIPA buffer containing phosphatase and protease inhibitors. After quantification by using BCA assay (Biosharp, BL521A), protein extract were used for western blotting according to a standard protocol. Primary antibodies against EZH2 (1:2000), H3K27me3 (1:1000), H3 (1:1000), PPARγ (1:1000), CTGF (1:1000), pSMAD2/3 (1:1000), SMAD2/3 (1:1000), GAPDH (1:2000) were used. Details of the antibodies were listed in Table 1. The intensity of the protein bands was analyzed by ImageJ software (Media Cybernetics, Bethesda, MD, USA) using GAPDH as the reference protein.

2.12. Chromatin immunoprecipitation (ChIP) assay

The ChIP analysis was performed using the SimpleChIP Plus Enzymatic Chromatin IP Kit (Cell Signaling Technology, #9005). Briefly, cells were crosslinked with 1 % formaldehyde for 10 min and lysed. Chromatin was digested and then fragmented by sonication. Immunoprecipitation was performed using antibodies against H3K27me3 (Cell Signaling Technology, #9733) and isotype control IgG (Cell Signaling Technology, #2729). Then, qPCR was performed to amplify the corresponding binding site. Based on previous studies [37,38], primers for PPARγ gene were 3′ exon specific. The sequences were as follows: 5′-AAATGCCTTGCAGTGGGGAT -3' (sense) and 5′-ATCTCCGCCAACAGCTTCTC -3' (antisense). Each qPCR reaction was performed in triplicate. Sample values were normalized to the average values of inputs.

2.13. Statistics

Data are expressed as means ± standard deviation (SD). Error bars in the charts represent SD. Statistically significant differences between 2 groups were established using 2-tailed Student's t test. Statistical significance among 3 or more groups was established using one-way ANOVA and Tukey's post hoc tests. Significance was set at $P < 0.05$. Data were analyzed and graphically presented using GraphPad Prism software (V10, San Diego, CA, USA).

Table 2
Primer sequence for RT-qPCR experiment.

Gene	Sequence
COL1A1-F	5′-GATTCCCTGGACCTAAAGGTGC-3′
COL1A1-R	5′-AGCCTCTCCATCTTTGCCAGCA-3′
FN1-F	5′-ACAACACCGAGGTGACTGAGAC-3′
FN1-R	5′-GGACACAACGATGCTTCCTGAG-3′
CTGF-F	5′-CTTGCGAAGCTGACCTGGAAGA-3′
CTGF-R	5′-CCGTCGGTACATACTCCACAGA-3′
αSMA-F	5′-AGGTCATCACCATCGGCAACGA-3′
αSMA-R	5′-GCTGTTGTAGGTGGTCTCGTGA-3′
EZH2-F	5′-GTACACGGGGATAGAGAATGTGG-3′
EZH2-R	5′-GGTGGGCGGCTTTCTTTATCA-3′
PPARG-F	5′-AGCCTGCGAAAGCCTTTTGGTG-3′
PPARG-R	5′-GGCTTCACATTCAGCAAACCTGG-3′

F: Forward; R: Reverse.

3. Results

3.1. EZH2 and H3K27me3 level were upregulated in lymphedema fibroadipose tissue

Lymphedema is characterized by fibroadipose tissue deposition at the advanced stage [39]. In total 5 lymphedema skin tissue and 3 normal control skin tissue were collected. As shown in H&E staining, obvious collagen fibers were found in lymphedema tissue, while normal subcutaneous tissue was mainly adipose tissue (Fig. 1A). Picrosirius red and Masson's Trichome staining verified the significant fibrosis in lymphedema tissue (Fig. 1B and C). Fibrotic marker genes, including *COL1A1*, *FN1*, *CTGF* and *αSMA*, significantly increased in lymphedema tissue when compared to normal tissue (Fig. 1D). These results were consistent with previous studies on the fibroadipose pathogenesis of lymphedema. Building upon the establish role of EZH2 in fibrotic disorders, we then examined the level of EZH2 and H3K27me3, through which EZH2 mediated transcriptional silencing [22–29]. RT-qPCR result showed significant elevated expression of *EZH2* (Fig. 1E). Immunofluorescence staining demonstrated the upregulation of EZH2 and H3K27me3 in lymphedema tissue (Fig. 1F–I). High magnification images showed that the elevated EZH2 was in the nucleus, inducing the trimethylation of histone H3 (H3K27me3). Co-staining of EZH2, H3K27me3 and αSMA verified that the upregulated EZH2 and H3K27me3 are mainly localized in αSMA positive cells, supporting the potential role of EZH2-mediated H3K27me3 modification in regulating fibrogenesis (Fig. S1).

3.2. EZH2 inhibition alleviates the fibrosis in mouse secondary lymphedema model

Considering the possible role of EZH2 in the fibrosis progression of lymphedema, we examined the therapeutic effects of EZH2 inhibitors. The small molecule inhibitors EPZ6438 and GSK126 inhibit EZH2 through competitive inhibition with S-adenosy-L-methionine (SAM), which is required for EZH2 function [32]. We established the mouse hind limb secondary lymphedema model in male mice and treated the mice with EZH2 inhibitors (Fig. 2A). The treatment didn't affect the other organs of the mice (Fig. S1). Based on H&E staining, lymphadenectomy (LN) surgery caused the fibroadipose tissue deposition in the hindlimb (Fig. 2B). After treated with EZH2 inhibitors, the overall skin thickness, epidermis thickness and fibroadipose tissue thickness were significantly decreased (Fig. 2E–G). Picrosirius red and Masson's

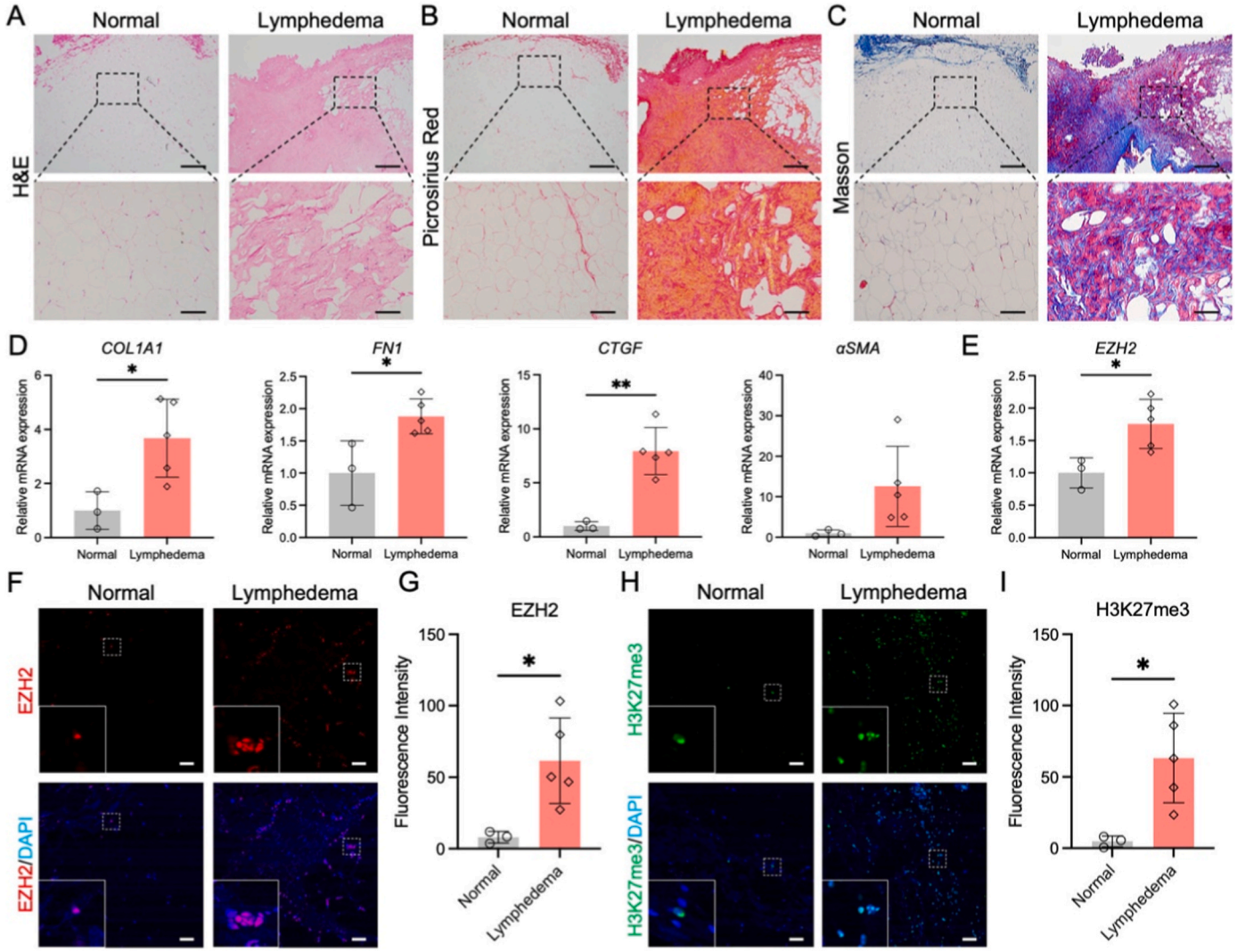

Fig. 1. EZH2 and H3K27me3 level were upregulated in secondary lymphedema fibroadipose tissue. (A–C) H&E, picrosirius red and Masson's trichrome staining of human subcutaneous tissue, scale bars: upper panel: 500 μm, lower panel: 100 μm (n = 3 for normal, n = 5 for lymphedema). (D–E) Expression levels of fibrogenic genes including *COL1A1*, *FN1*, *CTGF*, *αSMA* and *EZH2* in human tissue (n = 3 for control, n = 5 for lymphedema). (F–I) Immunofluorescence staining and quantitative analysis of EZH2 and H3K27me3 in human subcutaneous tissue, scale bar: 50 μm (n = 3 for normal, n = 5 for lymphedema). The data are expressed as means ± SD. Statistical significance is established using 2-tailed Student's t test, $^{*}P < 0.05$, $^{**}P < 0.01$.

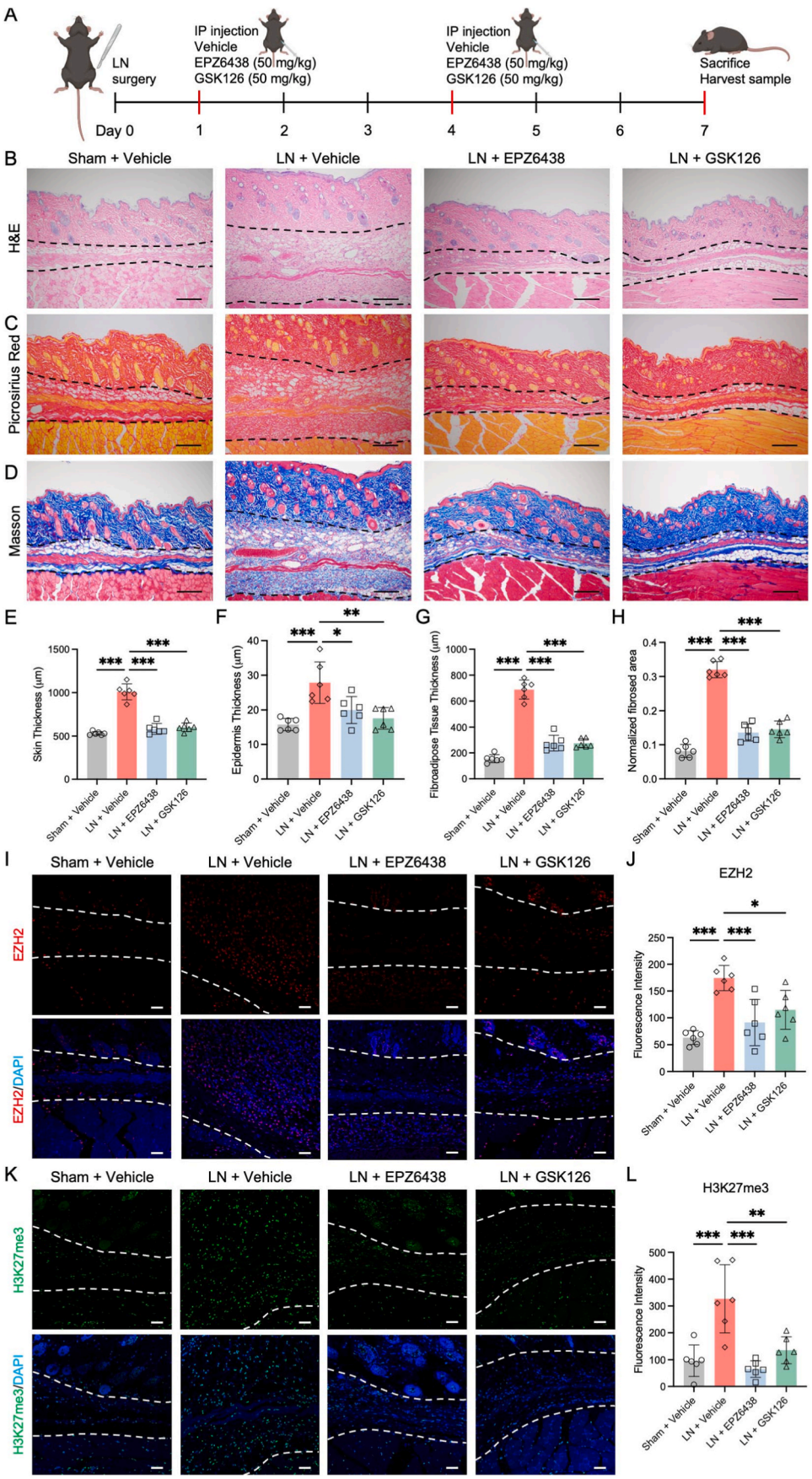

(caption on next page)

Fig. 2. EZH2 inhibition alleviates the fibroadipose tissue deposition in mouse secondary lymphedema model. (A) Schematic illustration of the animal study design. (B–D) H&E, picrosirius red and Masson's trichrome staining of mouse skin tissue, scale bar: 200 μm (n = 6 per group). (E–H) Quantification of overall hind limb skin thickness, epidermis thickness, fibroadipose tissue thickness and fibrosed area (n = 6 per group). (I–J) Immunofluorescence staining and quantitative analysis of H3K27me3 in mouse skin tissue, scale bar: 50 μm (n = 6 per group). (K–L) Immunofluorescence staining and quantitative analysis of H3K27me3 in mouse skin tissue, scale bar: 50 μm (n = 6 per group). The data are expressed as means ± SD. Statistical significance is established using one-way ANOVA and Tukey's post hoc tests, $^{*}P < 0.05$, $^{**}P < 0.01$, $^{***}P < 0.001$.

Trichome staining were used to assess fibrosis (Fig. 2C and D). We noted a significant reduction of fibrosed area in EZH2 inhibitors treated groups (Fig. 2H). Similar results were found in female mice (Fig. S3). Immunofluorescence staining verified the upregulation of EZH2 and H3K27me3 level in mice with lymphedema, while their levels were significantly reduced in EZH2 inhibitors treated mice (Fig. 2I–L).

3.3. EZH2 inhibition inhibited fibrogenic differentiation of AdMSCs

Fibrosed tissue accumulation in advanced lymphedema arises from pathological fibrogenic differentiation of AdMSCs, characterized by excessive extracellular matrix (ECM) secretion. To investigate EZH2's regulatory role, we established an *in vitro* fibrogenesis model using TGFβ1-stimulated human AdMSCs. TGFβ1 induced fibrogenic differentiation, evidenced by upregulation of CTGF (Fig. 3A–D) and increased expression of fibrotic marker genes (*COL1A1*, *FN1*, *CTGF* and *αSMA*) (Fig. 3E). We noticed that EZH2 and H3K27me3 level were also upregulated after TGFβ1 treatment (Fig. 3A–D). Next, we performed cytotoxicity assays for EZH2 inhibitors in the *in vitro* experiments. Based on the CCK-8 assays performed on different concentrations and different time points, 5 μM EPZ6438 and 2 μM GSK126 were used for the *in vitro* studies (Fig. 3F). Treatment with EZH2 inhibitors for 48 h effectively reverse the TGFβ1-induced changes. H3K27me3 level and fibrogenic marker CTGF induced by TGFβ1 was downregulated after EZH2 inhibitors treatment (Fig. 3C and D). Real-time PCR results verified the inhibition of fibrotic marker genes (*COL1A1*, *FN1*, *CTGF* and *αSMA*) in EZH2 inhibitors-treated AdMSCs (Fig. 3E). These results revealed that inhibition of EZH2 efficiently inhibited fibrogenic differentiation of AdMSCs.

3.4. PPARγ signaling was inhibited in lymphedema tissue

To explore how EZH2 affected the fibrosis progress, RNA sequencing was carried out on lymphedema (n = 5) and normal (n = 3) subcutaneous tissue to find possible involved signaling pathways. Lymphedema tissue had different transcriptional profile compared to normal tissue (Fig. 4A). A total of 2025 genes were found to be significantly upregulated, while 1285 genes were downregulated in lymphedema tissue (Fig. 4B). Functional enriched pathways of differentially expressed genes in KEGG included metabolic pathways, regulation of lipolysis in adipocytes, ECM-receptor interaction etc (Fig. 4C). Among them, PPAR signaling pathway was significantly enriched ($P < 0.0001$). GSEA result further indicated that PPAR signaling was inhibited in lymphedema tissue (Fig. 4D). Studies have shown that PPAR signaling pathway was involved in the fibrosis process [40,41]. Our previous study revealed that PPARγ agonist treatment reduced the fibrosis in the mouse secondary lymphedema model [33]. Here, we found the expression level of PPARG was downregulated in human lymphedema tissue (Fig. 4E), providing further evidence of the important role of PPARγ signaling in lymphedema fibrosis progress.

3.5. EZH2 inhibition activated PPARγ signaling

Next, we examined whether EZH2 inhibition activated PPARγ signaling *in vivo* and *in vitro*. Immunofluorescence staining showed increased expression of PPARγ in EZH2 inhibitors treated mice (Fig. 5A and B). Similarly, EZH2 inhibitors treatment induced the expression level of *PPARG*, which was inhibited by TGF-β1 in AdMSCs (Fig. 5C). Western blot showed a similar result (Fig. 5D and E). To delineate the epigenetic regulation of PPARγ by EZH2-mediated H3K27me3, we performed ChIP assay with anti-H3K27me3 antibody or control IgG. Consistent with previous studies [37,38], our result revealed the enrichment of H3K27me3 in the 3' exons of PPARγ, leading to the gene transcriptional silencing (Fig. 5F). Prior studies have shown that activating PPARγ signaling effectively counteracted TGFβ-SMAD2/3 signaling, which is crucial to fibrogenesis [42,43]. Immunofluorescence staining demonstrated the reduction of pSMAD2/3 in the hind limb of EZH2 inhibitor treated mice (Fig. 5G and H).

3.6. PPARγ signaling activation was essential for anti-fibrotic effect of EZH2 inhibition

To delineate the PPARγ-dependent anti-fibrotic mechanism of EZH2 inhibition, we implemented rescue experiments by using GW9662, a selective antagonist of PPARγ. While EZH2 inhibitors induced the upregulation of PPARγ, GW9662 inhibited PPARγ signaling (Fig. 6A–C). More importantly, GW9662 administration reversed the EZH2 inhibition-mediated suppression of CTGF protein expression without altering H3K27me3 level, which was significantly inhibited by EZH2 inhibitors (Fig. 6D and E). Inhibition of TGFβ-SMAD2/3 pathway by EZH2 inhibitors was also reversed by the use of GW9662 reflected by the upregulation of pSMAD2/3 (Fig. 6D and E). Similar results were found across the key fibrotic marker genes (*COL1A1*, *FN1*, *CTGF* and *αSMA*) by RT-qPCR (Fig. 6F). Administration of GW9662 *in vivo* also reversed the anti-fibrotic effect of EPZ6438 (Fig. S4). These results illustrated that EZH2 inhibition attenuates fibrosis via activating PPARγ signaling (Fig. 7).

4. Discussion

The present study establishes EZH2 upregulation as a hallmark of fibroadipose deposition in secondary lymphedema. Pharmacological EZH2 inhibition by EPZ6438 and GSK126 show therapeutic efficacy in the fibroadipose pathogenesis of secondary lymphedema model *in vivo*, and inhibit fibrogenic differentiation of AdMSCs induced by TGFβ1 *in vitro*. Mechanistically, we delineate a EZH2-H3K27me3-PPARγ axis wherein EZH2 inhibition induced PPARγ signaling, which in turn suppresses canonical TGFβ-SMAD2/3 signaling. This inhibition explains the anti-fibrotic efficacy of EZH2 inhibitors, providing a new strategy for the treatment of secondary lymphedema.

Our findings align with emerging reports of EZH2-mediated fibrosis across multiple systems. Du et al. showed EZH2-mediated H3K27me3 downregulated Krüppel-like factor 14 (KLF14), activated hepatic stellate cells and exerted a critical role in liver fibrogenesis [22]. By using EPZ6438 and UNC1999, Lee et al. found these EZH2 inhibitors reduced inflammatory cytokines (interleukin 1β, interleukin 6, interferon γ) and fibrosis markers (TGFβ, CTFF, COL1A1) in non-alcoholic steatohepatitis mice [23]. Xiao et al. reported that EZH2 induced the differentiation of fibroblasts to myofibroblasts in pulmonary fibrosis by enhancing SMAD2/3 nuclear translocation [24]. In acute respiratory distress syndrome (ARDS)-associated pulmonary fibrosis, EZH2 inhibition was reported to ameliorate fibroproliferation and regulate macrophage polarization [25]. Similarly, Zhou et al. revealed that EZH2 activated M2 macrophage polarization and promotes renal fibrosis [26]. Besides, EZH2 was also involved in the cardiac and peritoneal fibrosis [27–29]. Our study extends the potential utility of EZH2 inhibitors to the context

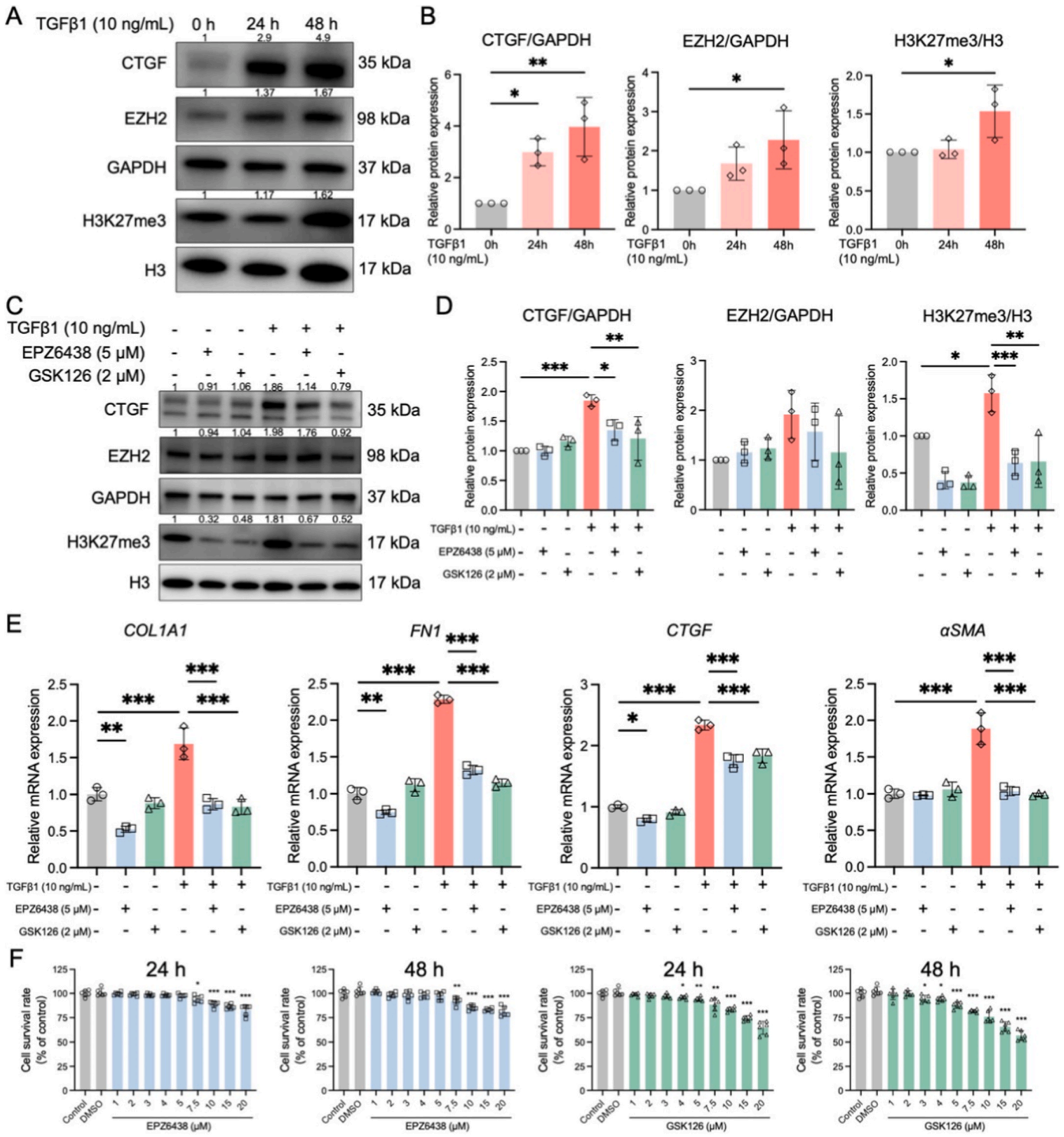

Fig. 3. EZH2 inhibition inhibited fibrogenic differentiation of AdMSCs. (A–B) Protein levels and quantitative analysis of CTGF, EZH2, GAPDH, H3K27me3 and H3 in TGFβ1 treated AdMSCs (n = 3). (C–D) Protein levels and quantitative analysis of CTGF, EZH2, GAPDH, H3K27me3 and H3 in TGFβ1 stimulated AdMSCs treated with/without EZH2 inhibitors (n = 3). (E) Expression levels of fibrogenic genes including *COL1A1*, *FN1*, *CTGF* and *αSMA* in TGFβ1 stimulated AdMSCs treated with/without EZH2 inhibitors (n = 3). (F) CCK-8 assays on different concentrations of EPZ6438 and GSK126 at 24 h and 48 h in AdMSCs (n = 6). The data are expressed as means ± SD. Statistical significance is established using one-way ANOVA and Tukey's post hoc tests, $^{*}P < 0.05$, $^{**}P < 0.01$, $^{***}P < 0.001$.

of skin fibroadipose pathogenesis in secondary lymphedema.

Functional enrichment of our RNA-seq data showed PPAR signaling was significantly enriched. We have reported that activating PPARγ, a key regulator in PPAR signaling, can reduce fibroadipose tissue in secondary lymphedema [33]. Here, we identified that EZH2 is the upstream of PPARγ signaling. Hu et al. reported weak enrichment of H3K27me3 in the promoter of *PPARG*, but knockdown of EZH2 also led to a significant upregulation of *PPARG* [37]. Mann et al. revealed that EZH2, stimulated by methyl-CpG binding protein 2 (MeCP2), methylated H3K27 to form a repressive chromatin structure in the 3' exons of PPARγ, negatively regulated PPARγ transcription in myofibroblasts [38]. Activation of TGFβ-SMAD2/3 signaling pathway is involved in the pathological

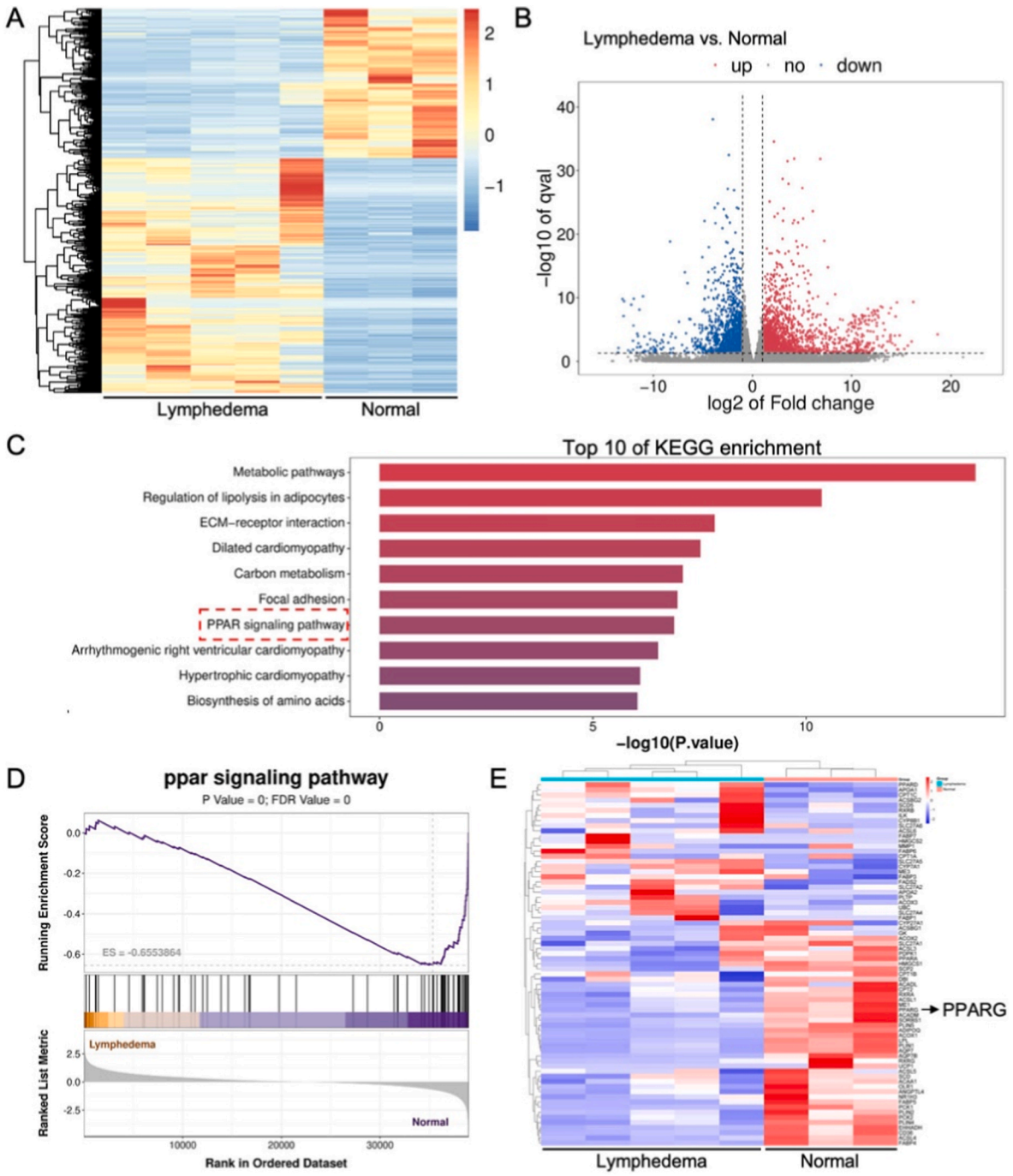

Fig. 4. PPARγ signaling was inhibited in secondary lymphedema fibroadipose tissue. (A) Heatmap of the differentially expressed genes from RNA sequencing analysis in human subcutaneous tissue, red and blue color indicate upregulation and downregulation, respectively (n = 3 for normal, n = 5 for lymphedema). (B) Volcano plots of differentially expressed genes from RNA sequencing analysis, red, blue and gray represent upregulation, downregulation, and non-significant, respectively. (C) Functional enriched pathways of differentially expressed genes in KEGG. (D) Gene set enrichment analysis (GSEA) for PPAR signaling pathway. (E) Heatmap of the differentially expressed genes in PPAR signaling pathway (n = 3 for normal, n = 5 for lymphedema).

cascade leading to excessive extracellular matrix deposition and fibroblast differentiation [19]. PPARγ has been well established as a negative regulator of the TGFβ-SMAD2/3 signaling and fibrotic markers [43–47]. These studies support our findings. Our results revealed that EZH2 is a upstream regulator of TGFβ-SMAD2/3 signaling via repressing the expression of PPARγ.

Secondary lymphedema has traditionally been recognized as a complication of cancer therapies, especially following lymph node dissection or radiation. Emerging evidence further highlights the association between secondary lymphedema and orthopedic diseases and treatment, including comminuted fractures with soft tissue compromise, iatrogenic lymphatic disruptions during procedures like musculoskeletal tumor resection and total joint arthroplasty [5–7]. Mechanistically, post-traumatic inflammation, surgical intervention and prolonged immobilization may exacerbate lymphatic dysfunction [48]. Many orthopaedic surgeons pay attention to the risk assessment, prevention, and early management of secondary lymphedema. Current surgical treatment of lymphedema was performed by orthopedic doctors, underscoring the necessity for multidisciplinary strategies to address the etiology of secondary lymphedema. More and more orthopaedic doctors

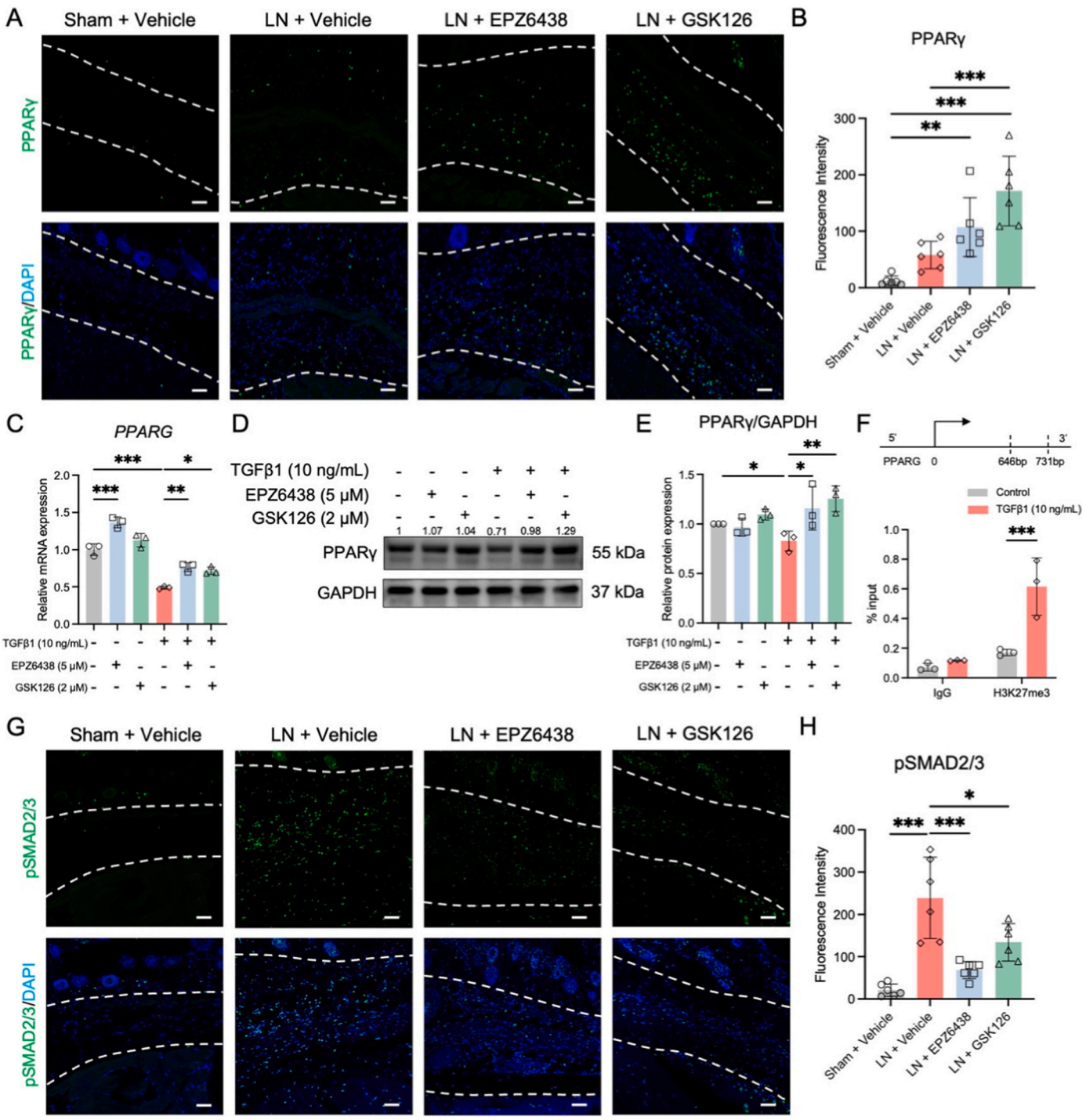

Fig. 5. EZH2 inhibition induced PPARγ signaling and inhibited TGFβ-SMAD2/3 signaling. (A–B) Immunofluorescence staining and quantitative analysis of PPARγ in mouse skin tissue, scale bar: 50 μm (n = 6 per group). (C) Expression levels of *PPARG* in TGFβ1 stimulated AdMSCs treated with/without EZH2 inhibitors (n = 3). (D–E) Protein levels and quantitative analysis of PPARγ in TGFβ1 stimulated AdMSCs treated with/without EZH2 inhibitors (n = 3). (F) ChIP assay for IgG and H3K27me3, and subsequent qPCR in PPARγ 3′ exon, IgG as a negative control (n = 3). (G–H) Immunofluorescence staining and quantitative analysis of pSMAD2/3 in mouse skin tissue, scale bar: 50 μm (n = 6 per group). The data are expressed as means ± SD. Statistical significance is established using one-way ANOVA and Tukey's post hoc tests, $^{*}P < 0.05$, $^{**}P < 0.01$, $^{***}P < 0.001$.

are expecting novel strategies to treat lymphedema instead of performing operations such as vascularized lymph node transfer and liposuction. Our findings redefine secondary lymphedema fibroadipose deposition as an epigenetic disorder. Epigenetic drugs can reset pathogenic epigenetic states while preserving genomic integrity. Early epigenetic intervention during the lymphatic compensatory phase may break the self-perpetuating fibrosis cycle, which impairs lymphatic circulation and exacerbates fibrosis. Several epigenetic drugs have been approved for clinical application. Tazemetostat (EPZ6438) is a potent, selective and orally available EZH2 inhibitor, which has been approved by FDA for adult patients with relapsed or refractory follicular lymphoma [31,32]. Valemetostat, a dual inhibitor of EZH1 and EZH2, is approved in Japan to treat adult T-cell leukemia/lymphoma [49]. Our study provide a theoretical foundation for expanding the clinical

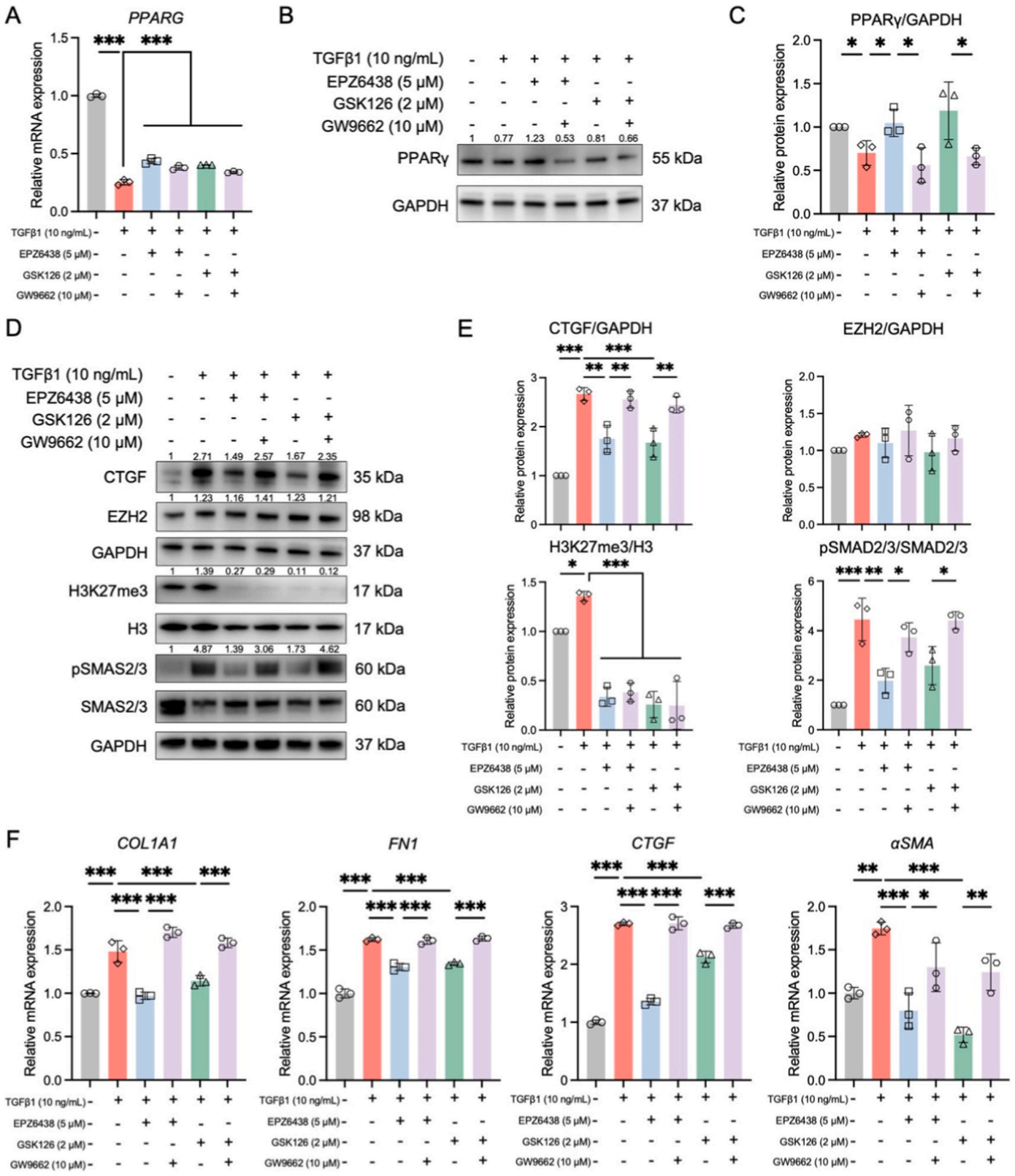

Fig. 6. PPARγ antagonist GW9662 reversed EZH2 inhibition-mediated anti-fibrotic effect. (A) Expression levels of *PPARG* in TGFβ1 stimulated AdMSCs treated with/without EZH2 inhibitors and GW9662 (n = 3). (B–C) Protein levels and quantitative analysis of PPARγ in TGFβ1 stimulated AdMSCs treated with/without EZH2 inhibitors and GW9662 (n = 3). (D–E) Protein levels and quantitative analysis of CTGF, EZH2, GAPDH, H3K27me3, H3, pSMAD2/3 and SMAD2/3 in TGFβ1 stimulated AdMSCs treated with/without EZH2 inhibitors and GW9662 (n = 3). (F) Expression levels of fibrogenic genes including *COL1A1*, *FN1*, *CTGF* and *αSMA* in TGFβ1 stimulated AdMSCs treated with/without EZH2 inhibitors and GW9662 (n = 3). The data are expressed as means ± SD. Statistical significance is established using one-way ANOVA and Tukey's post hoc tests, $^{*}P < 0.05$, $^{**}P < 0.01$, $^{***}P < 0.001$.

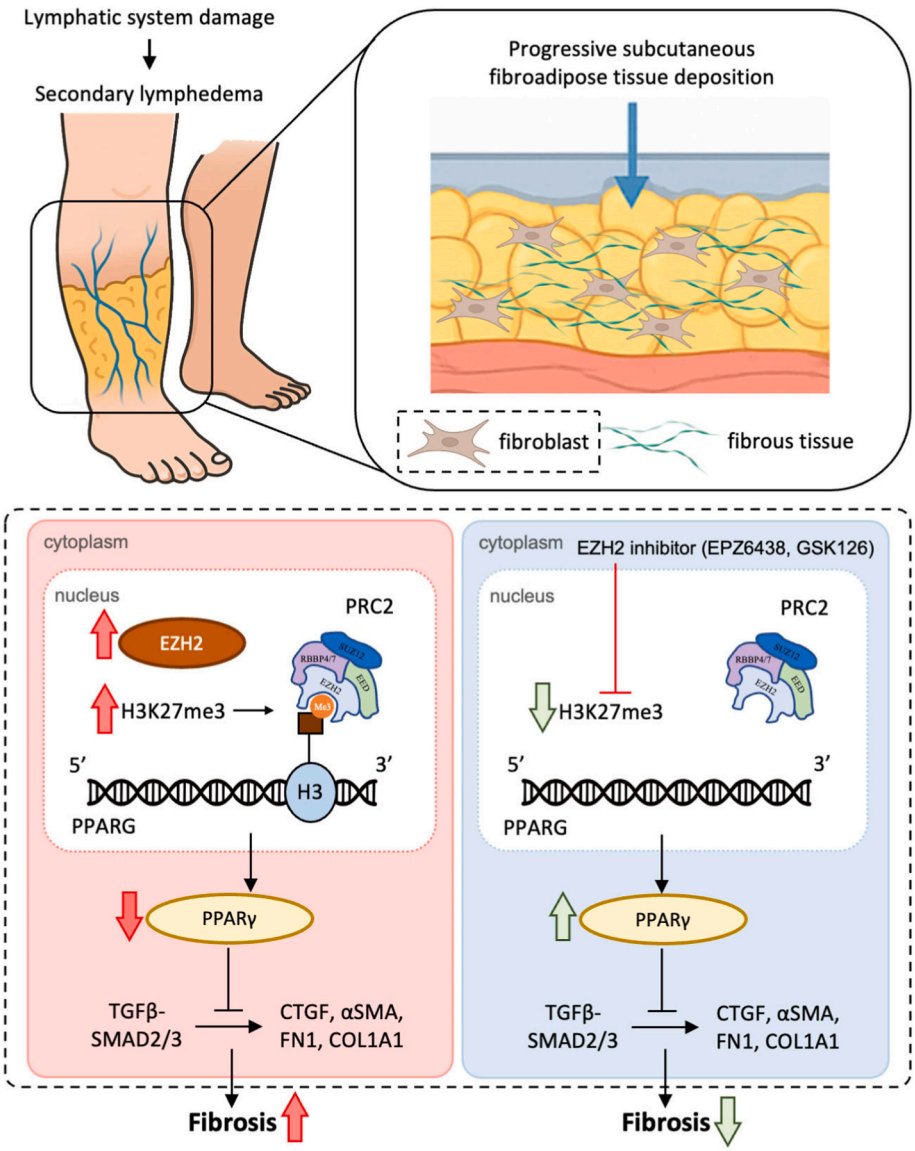

Fig. 7. Schematic illustration of the mechanism by which EZH2 inhibition attenuates fibrosis via activating PPARγ signaling.

indications of EZH2 inhibitors. This pharmacotherapy can be administered in combination with conventional decongestive therapy and surgical approaches, presenting a promising strategy to achieve better outcomes.

For cancer patients, existing EZH2 inhibitors are administered orally. Long-term systemic administration of EZH2 inhibitors may cause the disruption of immune and metabolic homeostasis [50]. For lymphedema patients, local delivery strategies including hydrogel, nanoparticle-based systems and microneedles are available options. The dosage of EZH2 inhibitor needed for lymphedema treatment may also be different from cancer treatment. Future research should be focused on local delivery strategies and optimizing the dosage of EZH2 inhibitor in secondary lymphedema treatment.

There are also some limitations in this study. Firstly, while our murine model recapitulates human fibroadipose pathology, it lacks the chronic lymphatic insufficiency characteristics observed in advanced lymphedema. Secondly, the pleiotropic effects of EZH2 inhibitors on immune cells remain uncharacterized. Thirdly, despite the results of this study and those of other investigation have not revealed adverse effects on other organs [26], the optimization of local delivery strategies for EZH2 inhibitors need further development to avoid systemic administration. Lastly, our current results support a therapeutic role for EZH2 inhibition in lymphedema-specific tissue changes, rather than all types of skin edema. Further studies are warranted to explore the potential efficacy of EZH2 inhibitors in models of non-lymphatic skin edema.

5. Conclusion

This study establishes EZH2 as the pivotal factor in the fibroadipose pathogenesis of secondary lymphedema, wherein its activity suppress PPARγ. By elucidating that epigenetic reprogramming by EZH2 inhibition can effectively inhibit fibrosis, we present a strategy for the development of disease-modifying therapy for fibrotic disorder in secondary lymphedema.

Author contributions

Conceptualization: Ziyu Chen, Shailesh Agarwal, Ye Li, Lixiang Xue, Deli Wang. Methodology: Ziyu Chen, Zhi Yao, Mengfan Wu, Yuluan Wu, Jianlin Zhang, Zhuangyao Liao, Junyu Qian, Jiewen Wei. Investigation: Ziyu Chen, Zhi Yao, Mengfan Wu, Yuluan Wu, Jianlin Zhang, Zhuangyao

Liao, Junyu Qian, Jiewen Wei, Lili Song, Longbiao Yu, Jingjing Wen, Zhegang Zhou, Yihao Wei, Yuefeng Yao, Zetao Ma, Pei Liu. Visualization: Ziyu Chen, Zhi Yao, Mengfan Wu. Funding acquisition: Ziyu Chen, Zhi Yao, Mengfan Wu, Deli Wang. Project administration: Ziyu Chen, Shailesh Agarwal, Ye Li, Lixiang Xue, Deli Wang. Supervision: Shailesh Agarwal, Ye Li, Lixiang Xue, Deli Wang. Writing – original draft: Ziyu Chen, Zhi Yao, Mengfan Wu, Shailesh Agarwal, Ye Li, Lixiang Xue, Deli wang. Writing – review & editing: Ziyu Chen, Zhi Yao, Mengfan Wu, Jianlin Zhang, Shailesh Agarwal, Ye Li, Lixiang Xue, Deli wang. All authors approved the final version.

Funding sources

This work was supported by the National Nature Science Foundation of China (82404113, 82402802, 82302810), Basic and Applied Basic Research Foundation of Guangdong Province (2023A1515111068, 2023A1515220250), China Postdoctoral Science Foundation (2023M742390), Shenzhen Science and Technology Program (JCYJ20230807095121041, JCYJ20230807095203007, JCYJ20220531094004010, RCBS20231211090537061), Scientific Research Foundation of Peking University Shenzhen Hospital (KYQD2023244, KYQD2023245), Shenzhen Key Medical Discipline Construction Fund (SZXK023), Sanming Project of Medicine in Shenzhen (SZSM202211038), Shenzhen High-level Hospital Construction Fund.

Declaration of competing interest

The authors declare that they have no known competing financial interests or personal relationships that could have appeared to influence the work reported in this paper.

Appendix A. Supplementary data

Supplementary data to this article can be found online at https://doi.org/10.1016/j.jot.2025.08.014.

Data availability

The data supporting the findings are presented in the article and supplementary materials, further inquiries can be directed to the corresponding author.

References

[1] Alitalo K, Tammela T, Petrova T. Lymphangiogenesis in development and human disease. Nature 2005;438(7070):946–53.
[2] Jiang X, Nicolls M, Tian W, Rockson S. Lymphatic dysfunction, leukotrienes, and lymphedema. Annu Rev Physiol 2018;80:49–70.
[3] The diagnosis and treatment of peripheral lymphedema: 2020 consensus document of the international society of Lymphology. Lymphology 2020;53(1):3–19.
[4] Ayman AG, Tania J, Lymphedema P. Pathophysiology and clinical manifestations. J Am Acad Dermatol 2017;77(6).
[5] Banasiak S, Hartel M, Frosch K, Berger-Groch J. Postoperative lymphedema after primary total hip arthroplasty: prospective analysis of bikini incision-type direct anterior approach versus established standard approaches. J Orthop Surg Res 2024;19(1):54.
[6] Medin Ceylan C, Ersoy S, Kesiktas F, Özokur A. Demonstration of the effectiveness of complete decongestive treatment in secondary lymphedema developing after total knee arthroplasty. European journal of orthopaedic surgery & traumatology : Orthop Traumatol 2024;35(1):45.
[7] Zheng Y, Wang P, Zhao L, Xing L, Xu H, Li N, et al. A novel therapy for fracture healing by increasing lymphatic drainage. Journal of orthopaedic translation 2024;45:66–74.
[8] Mahmoud Hamada M, Rafik E R, Mohamed ME, Abdelrazak A, Hend R, S, et al. The impact of lymphedema severity on shoulder joint function and muscle activation patterns in breast cancer survivors: a cross-sectional study. Support Care Cancer 2024;33(1).
[9] Laura G, Kim L, Claire C, Linda KD. Effectiveness of complete decongestive therapy for upper extremity breast cancer-related lymphedema: a review of systematic reviews. Med Oncol 2024;41(11).
[10] Shelley D, Claire C D, Laura G, Kim L, Marie-Eve L, Amy R, et al. Complete decongestive therapy phase 1: an expert consensus document. Med Oncol 2024;41(12).
[11] Elisabeth A K, Adriano F, Florian S H, Alina A-G, Julia S, Birgit A-F, et al. Vascularized lymph node transfer (VLNT) versus lymphaticovenous anastomosis (LVA) for chronic breast cancer-related lymphedema (BCRL): a retrospective cohort study of effectiveness over time. Breast Cancer Res Treat 2024;(0).
[12] Sai Anusha S, Sophia C, Rachel AA, Justin MS. Advances in surgical management of chronic lymphedema: current strategies and future directions. Med Oncol 2025;42(2).
[13] Ann Marie F, Mei Rosemary F, Karen J B, Elizabeth C, Kathleen F, Corinne K, et al. Post-operative care for patients following surgical treatment of lymphedema. Med Oncol 2024;41(11).
[14] Kataru R, Wiser I, Baik J, Park H, Rehal S, Shin J, et al. *Fibrosis and secondary lymphedema: chicken or egg?* Translational research. J Lab Clin Med 2019;209:68–76.
[15] Brown S, Dayan J, Kataru R, Mehrara B. The vicious circle of stasis, inflammation, and fibrosis in lymphedema. Plast Reconstr Surg 2023;151(2):330e–41e.
[16] Nakamura K, Radhakrishnan K, Wong Y, Rockson S. Anti-inflammatory pharmacotherapy with ketoprofen ameliorates experimental lymphatic vascular insufficiency in mice. PLoS One 2009;4(12):e8380.
[17] Gardenier J, Kataru R, Hespe G, Savetsky I, Torrisi J, Nores G, et al. Topical tacrolimus for the treatment of secondary lymphedema. Nat Commun 2017;8:14345.
[18] Sang-Oh L, Il-Kug K. Molecular pathophysiology of secondary lymphedema. Front Cell Dev Biol 2024;12 (0).
[19] Jung Eun B, Hyeung Ju P, Raghu PK, Ira LS, Catherine LL, Jinyeon S, et al. TGF-β1 mediates pathologic changes of secondary lymphedema by promoting fibrosis and inflammation. Clin Transl Med 2022;12(6).
[20] Mark AD, Tony K. Cancer epigenetics: from mechanism to therapy. Cell 2012;150(1).
[21] Singh P. Histone methyl transferases: a class of epigenetic opportunities to counter uncontrolled cell proliferation. Eur J Med Chem 2019;166:351–68.
[22] Du Z, Liu M, Wang Z, Lin Z, Feng Y, Tian D, et al. EZH2-mediated inhibition of KLF14 expression promotes HSCs activation and liver fibrosis by downregulating PPARγ. Cell Prolif 2021;54(7):e13072.
[23] Lee S, Woo D, Kang J, Ra M, Kim K, Lee S, et al. The role of the histone methyltransferase EZH2 in liver inflammation and fibrosis in STAM NASH mice. Biology 2020;9(5).
[24] Xiao X, Senavirathna L, Gou X, Huang C, Liang Y, Liu L. EZH2 enhances the differentiation of fibroblasts into myofibroblasts in idiopathic pulmonary fibrosis. Physiological reports 2016;4(17).
[25] Bao X, Liu X, Liu N, Zhuang S, Yang Q, Ren H, et al. Inhibition of EZH2 prevents acute respiratory distress syndrome (ARDS)-associated pulmonary fibrosis by regulating the macrophage polarization phenotype. Respiratory research 2021;22(1):194.
[26] Zhou X, Chen H, Hu Y, Ma X, Li J, Shi Y, et al. Enhancer of zeste homolog 2 promotes renal fibrosis after acute kidney injury by inducing epithelial-mesenchymal transition and activation of M2 macrophage polarization. Cell Death Dis 2023;14(4):253.
[27] Song S, Zhang R, Mo B, Chen L, Liu L, Yu Y, et al. EZH2 as a novel therapeutic target for atrial fibrosis and atrial fibrillation. Journal of molecular and cellular cardiology 2019;135:119–33.
[28] Ge Z, Yin C, Li Y, Tian D, Xiang Y, Li Q, et al. Long noncoding RNA NEAT1 promotes cardiac fibrosis in heart failure through increased recruitment of EZH2 to the Smad7 promoter region. J Transl Med 2022;20(1):7.
[29] Shi Y, Tao M, Wang Y, Zang X, Ma X, Qiu A, et al. Genetic or pharmacologic blockade of enhancer of zeste homolog 2 inhibits the progression of peritoneal fibrosis. J Pathol 2020;250(1):79–94.
[30] Michael TM, Heidi MO, Gopinath G, Susan K, Christine T, Glenn S VA, et al. EZH2 inhibition as a therapeutic strategy for lymphoma with EZH2-activating mutations. Nature 2012;492(7427).
[31] Makita S, Tobinai K. Targeting EZH2 with tazemetostat. Lancet Oncol 2018;19(5):586–7.
[32] Hoy S. Tazemetostat: first approval. Drugs 2020;80(5):513–21.
[33] Chen Z, Ghavimi S, Wu M, McNamara J, Barreiro O, Maridas D, et al. PPARγ agonist treatment reduces fibroadipose tissue in secondary lymphedema by exhausting fibroadipogenic PDGFRα+ mesenchymal cells. JCI insight 2023;8(24).
[34] Li Y, Wu M, Zhang Z, Xia J, Wang Z, Chen X, et al. Application of external force regulates the migration and differentiation of adipose-derived stem/progenitor cells by altering tissue stiffness. Tissue Eng 2019;25:1614–22. Part A.
[35] Tengrui Z, Zhengyang G, Xiao H, Yueqing G, Chen L, Jiaqi H, et al. Dysregulated lipid metabolism blunts the sensitivity of cancer cells to EZH2 inhibitor. EBioMedicine 2022;77 (0).
[36] Jiaqi H, Qianqian Y, Yuqing W, Xin Z, Yunyun G, Yuanjun T, et al. EZH2 inhibition enhances PD-L1 protein stability through USP22-mediated deubiquitination in colorectal cancer. Adv Sci (Weinh) 2024;11(23).
[37] Hu F, Chen H, Duan Y, Lan B, Liu C, Hu H, et al. CBX2 and EZH2 cooperatively promote the growth and metastasis of lung adenocarcinoma. Molecular therapy Nucleic acids 2022;27:670–84.
[38] Mann J, Chu D, Maxwell A, Oakley F, Zhu N, Tsukamoto H, et al. MeCP2 controls an epigenetic pathway that promotes myofibroblast transdifferentiation and fibrosis. Gastroenterology 2010;138(2):705–14. 714.e1-714.
[39] Rockson S, Keeley V, Kilbreath S, Szuba A, Towers A. Cancer-associated secondary lymphoedema. Nat Rev Dis Primers 2019;5(1):22.

[40] Son M, Kim G, Yang Y, Ha S, Kim J, Kim D, et al. PPAR Pan agonist MHY2013 alleviates renal fibrosis in a mouse model by reducing fibroblast activation and epithelial inflammation. Int J Mol Sci 2023;24(5).
[41] Boyer-Diaz Z, Aristu-Zabalza P, Andrés-Rozas M, Robert C, Ortega-Ribera M, Fernández-Iglesias A, et al. Pan-PPAR agonist lanifibranor improves portal hypertension and hepatic fibrosis in experimental advanced chronic liver disease. Journal of hepatology 2021;74(5):1188–99.
[42] Manzéger A, Garmaa G, Mózes M, Hansmann G, Kökény G. Pioglitazone protects tubular epithelial cells during kidney fibrosis by attenuating miRNA dysregulation and autophagy dysfunction induced by TGF-β. Int J Mol Sci 2023;24(21).
[43] Ghosh A, Bhattacharyya S, Wei J, Kim S, Barak Y, Mori Y, et al. Peroxisome proliferator-activated receptor-gamma abrogates Smad-dependent collagen stimulation by targeting the p300 transcriptional coactivator. FASEB J : official publication of the Federation of American Societies for Experimental Biology 2009; 23(9):2968–77.
[44] Heather FL, Thomas HT, R Matthew K, Tatiana M G, Richard P, Patricia JSP. The role of PPARs in lung fibrosis. PPAR Res 2007;2007 (0).
[45] Andréa Tavares D, Michelly Cristiny P, Moacyr Jesus Barreto dMR, Laurindo Ferreira Jr dR, Ivan da Rocha P, Cláudia Diniz Lopes M, et al. The role of PPAR gamma in systemic sclerosis. PPAR Res 2015;2015 (0).
[46] Anna M, Gantsetseg G, Miklós MM, Georg H, Gábor K. Pioglitazone protects tubular epithelial cells during kidney fibrosis by attenuating miRNA dysregulation and autophagy dysfunction induced by TGF-β. Int J Mol Sci 2023;24(21).
[47] Hazra S, Xiong S, Wang J, Rippe R, Krishna V, Chatterjee K, et al. Peroxisome proliferator-activated receptor gamma induces a phenotypic switch from activated to quiescent hepatic stellate cells. J Biol Chem 2004;279(12):11392–401.
[48] Trayes K, Studdiford J, Pickle S, Tully A. Edema: diagnosis and management. Am Fam Physician 2013;88(2):102–10.
[49] Dou F, Tian Z, Yang X, Li J, Wang R, Gao J. Valemetostat: first approval as a dual inhibitor of EZH1/2 to treat adult T-cell leukemia/lymphoma. Drug Discov Ther 2022;16(6):297–9.
[50] Renjing J, Jianlin Z, Yuqing W, Ziyu C, Xuan H, Xintong Z, et al. EZH2 in non-cancerous diseases: expanding horizons. Protein Cell 2025;16(9):764–81.